J. Mountain Res. P-ISSN: 0974-3030, E-ISSN: 2582-5011 DOI: https://doi.org/10.51220/jmr.v16i2.4
Vol. 16(2) Special Issue ICRAMS-2021, (2021), 21-34

Growth of ZnO nanorods array on PCB for enhanced UV photosensors

Ashish Yengantiwar[1*] And Arun Banpurkar[2]

1Department of Physics, Fergusson College (Autonomous), FC Road, Pune, Maharashtra, India, PIN: 411004

2Department of Physics, Savitribai Phule Pune University, Ganeshkhind, Pune, Maharashtra, India, PIN: 411007

*Corresponding Author Email id: ashish.yengantiwar@fergusson.edu

Received: 2.8.2021; Revised: 13.9.2021; Accepted: 20.9.2021

Abstract: Ultraviolet (UV) photosensitive device is fabricated using ZnO nanorods array on commercially available printed circuit board (PCB). Facile open aqueous solution deposition (OASD) method is used to deposit ZnO nanorods array in a trenched region between closely spaced Cu-electrodes. X-ray diffraction (XRD) patterns confirm the wurtzite phase of ZnO nanorods arrays and scanning electron microscopy (SEM) characterizes the multidimensional growth of ZnO nanorods across the trenched part of PCB. The current-voltage (I-V) characteristics of the device in dark is analogous to the back-to-back diode behaviour. However, the device exhibits an excellent photoresponsivity wherein the photocurrent value increases by two orders of magnitude at 2 V bias under the illumination ultraviolet (UV wavelength $\lambda \sim 254$ nm) light source. The enhancement in photocurrent is mainly due to formation of multiple contacts between neighbouring grain-boundaries of the nanorods arrays extending to the Cu-electrodes. The prototype optoelectronic device displays almost four-times increment in the UV photocurrent at 5 V external bias potential.

Keywords: ZnO nanorods, Cu-ZnO-Cu, UV Photoresponsivity, printed circuit board, solution deposition, back-to-back diode

Introduction:

Zinc oxide (ZnO) is II-VI wide band gap semiconducting metal oxide having direct-bandgap of ~ 3.2 to 3.3 eV (Chang et al 2007). Also, it has a high exciton binding energy of 60 meV, thus ZnO is a promising candidate for photonic devices in ultraviolet (UV) spectral range at normal operating temperature (Su et al 2010). Recently, quantum size effects and band gap engineering in ZnO nanostructures have demonstrated novel optoelectronic responses. Therefore, it is used in several devices such as a Schottky diode (Kao et al 2012), photodetector (Mandal et al 2012), photoemission (Huang et al 2001), field emission (Deo et al 2012), visible-blind UV photosensor ((Kao et al op cit) piezo-phototronic devices (Kumar et al 2019), heterojunction photodiode (Hwang et al 2020), humidity sensor (Farhat et al 2017), photoelectronic sensor (Chen et al 2017), UV sensors, biosensors, gas-sensors (Meng and Li 2020), Schottky-sensors (Wei et al 2009) and chemical sensor-based devices (Ahmad et al 2014), etc. More detailed survey on nanostructured devices using ZnO material has been found in comprehensive reviews (Consonni 2019, Özgür et al 2005, Zhai et al 2011). In general, nanobridging devices are based on lateral growth of suspended nanowires between prefabricated metal electrodes (Zhai et al 2011). It has been proved that metal-semiconductor-metal junction leads to either ohmic or Schottky

characteristics depending on their work function values (Brillson and Lu 2017). Most of the studies have reported a rectifying behaviour in the single or multiple nanorods bridge across trenched or interdigitated electrodes (Huang et al 2010, Ko et al 2015, Resmini et al 2015). On the other hand, non-linear current-voltage characteristic analogous to back-to back diode characteristics are often found in bulk and doped ZnO mainly used as high energy surge suppressor and protection devices (Mahan et al,1978, Mahan et al 1979)). In the previous study, pulsed laser deposited (PLD) thin films of ZnO also exhibit such non-linear I-V characteristics (Jejurikar et al 2006). In the present context, the growth of planar nanorod array by facile deposition is less explored. Also, in the planar-nanostructured array the lateral contacts provide large surface area and grain-boundary interconnects enables an added functionality like photoinduced current switching in the related devices (Bavelis et al 2014).

In the recent past, ZnO nanorods have been grown by various techniques including electrodeposition (Postels et al 2008), thermal evaporation (Umar et al 2006), metal organic chemical vapour deposition (MOCVD) (Ashraf et al 2011), vapour–liquid–solid growth method (VLS) (Li et al 2009), arc discharge method (Sönmezoğlu et al 2014), physical vapor deposition tecniques (Lyu et al 2003) etc. In this paper, we report UV photo-switchable planar ZnO NRs array on copper micro-trenched-electrode fabricated on commercial printed circuit board (PCB) to follow cost effective and simplistic design approach. In most of the previous studies, researchers have used conventional photolithography process for fabricating MSM UV detectors, which causes complex fabrication processes. Herein, the generic open aqueous solution deposition (OASD) technique is used to grow ZnO NRs in microtrenched Cu-electrode. This improved solution bath technique provides additional advantages such as convenient, fast growth, environment friendly reaction, control on growth parameters, uniform deposition on large substrate area, large-scale production of equivalent devices, low growth temperature, high reproducibility, and cost effectiveness (Yengantiwar et al 2011). All-solution approach that does not require any complex experimental apparatus and allows the fabrication of inexpensive self-assembled, multidimensional networks of ZnO nanorods. Such networks can be easily reproduced on interdigitated Cu- electrodes i.e., embedded metal-semiconductor-metal junction which exhibit UV-Photoswitchable varistor property, resulting directly in the development of very robust prototype devices.

Herein, we present the UV photo-responsive device which indicates the current-voltage (I-V) characteristics that are analogous to the back-to-back diode behaviour in dark conditions. However, it exhibits an excellent photoresponsivity where the photocurrent value increases by two orders of magnitude at 2 V bias under the illumination of ultraviolet (UV) light. The photoresponsivity and sensitivity values are estimated to be 0.25 A/W and 4, respectively. The temperature dependent electrical properties of devices reveal negative temperature coefficient of resistance effect above 370 K in the dark.

Materials and Methods:

Commercially available printed circuit board (PCB) of copper clad of thickness ~ 35 µm was etched by conventional photolithographic technique for obtaining the trenched copper electrode configuration. In total, 10 such trenched electrode devices were fabricated for ZnO nanorods deposition. Channels of these electrodes were 2 cm long and having 150 µm spacing between the electrodes. Thus, an active surface area of each Cu-clad was 2 × 0.0152 cm^2. Then substrates were thoroughly washed using detergent, ethanol, and distilled water in an ultrasonic bath for removal of dirt and oil traces if any. Finally, it was dried in nitrogen flow and loaded in the deposition cell of open aqueous solution bath. For the facile growth of ZnO nanorods, an equimolar (25 mM) solution of zinc nitrate and hexamethylene tetramine (HMT) was separately prepared using deionised water as solvent. At a time four substrates (Cu-clads) were mounted on Teflon holder and immersed into the solution maintained at equilibrium temperature 95 ˚C under slow stirring. The deposition was carried out for time duration of almost 3 hours. The sample substrates were taken out and rinsed several times with distilled water to wash away loosely attached ZnO NRs and later dried and checked for the electrical connectivity between electrodes. The above deposition process was carried out repeatedly to get an electrical connectivity between electrodes. Finally, the deposited substrates were vacuum dried at 70 ˚C and were used for structural and electrical characterizations. It is seen that ZnO NRs covers entire surface including copper electrodes and trenched area between electrodes. The deposition on copper layer remains practically inactive due to its short circuit contacts with underneath copper layer, therefore electrode masking becomes unimportant. Out of ten devices, eight were used for the electrical connection to copper surface by soldering another copper wire and remaining two samples were used for structural characterisation purposes.

X-ray diffraction (XRD) patterns were recorded at room temperature with Bruker Axis D8-Advance X-ray Diffractometer using Cu-K_α radiation (λ ~1.5406 Å). The morphology of device was characterized using Scanning Electron Microscopy (SEM) and elemental analysis was done with the help of energy dispersive X-ray spectroscopy (EDAX) operated at accelerating voltage range from 10 to 20 kV. UV-Vis absorbance spectra were obtained using Scan UV-Vis-NIR V-670 (Jasco) Spectrophotometer. The Photoluminescence (PL) spectra of the device were measured with LS-55 (Perkin Elmer) Spectrophotometer by using Xe lamp as excitation source at room temperature. UV light source peaked at wavelength λ ~ 254 nm (output power 8 W) was used for illumination of device. Electrical characterizations in dark and under UV illumination were performed using Keithley 2400-C source meter. Temperature-dependent electrical properties were also measured in dark.

Result and Discussion:

The XRD patterns of ZnO nanorods deposited copper electrode is shown in Fig.1 (a). The XRD clearly shows diffraction peaks corresponding to ZnO and Cu only, and absence of copper oxide

phases (JCPDS data PDF # 85-1326). It also shows that ZnO growth takes place in all the possible directions. However, line intensity ratios particularly (002) and (101) planes for the present case are 0.96 and standard powder sample (JCPDS data PDF # 79-0207) is 0.25 which indicates preferential growth along c-axis.

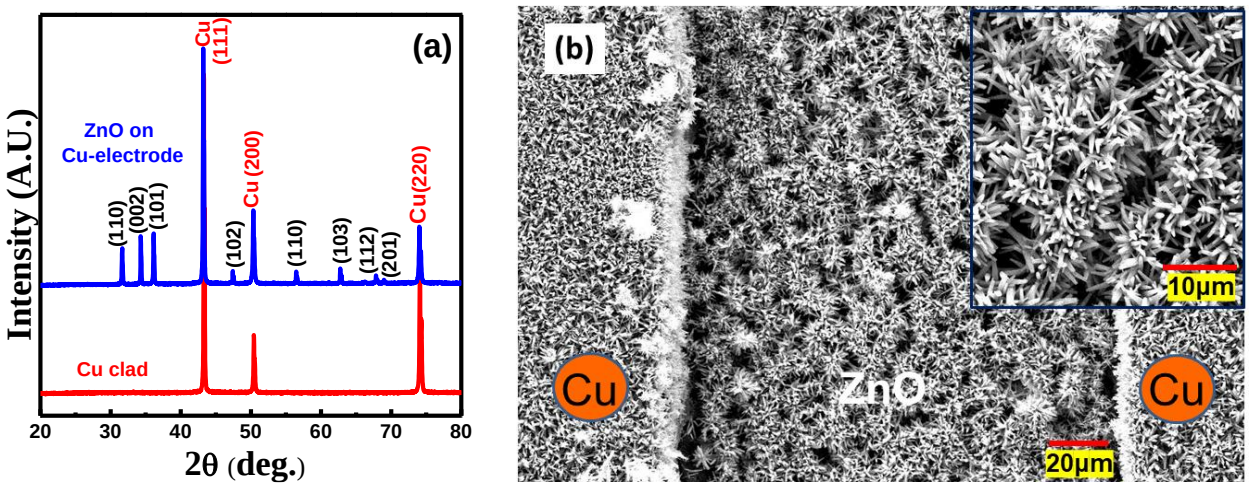

Fig. 1. (a) XRD pattern of the ZnO NRs growth on trenched Cu-electrodes and (b) SEM image of the ZnO NRs deposited between copper electrodes. The growth is also seen on Cu-electrodes, although the morphology differs. Inset (b) shows magnified image of ZnO NRs deposited on trenched part.

Fig. 1 (b) shows the growth morphology of ZnO NRs investigated using SEM. The formation of dense nanorods/nanoflowers over trenched region is observed. Moreover, prominent growth on copper electrode edges can be seen. The magnified image (inset) from a trenched region clearly illustrates interconnected ZnO NRs growth with flower and tree morphology. Specifically, the NRs growth takes place in the form of interconnected bushes/flowers spanning the space between copper–electrodes. Here electrical connections could be established only due to interconnected nanorods. Fig. also depicts that bushes/flowers provide high active surface area increases harvesting of incoming photon. Fig. 2 (a) illustrates the morphologies of ZnO NRs at the edge of the copper electrodes. ZnO Nanorods are densely packed at the edge of the copper electrode suitable for multiple interconnections with neighbouring nano-flower/trees. ZnO NRs morphology at the electrode edges provides excellent contacts between electrodes and ZnO flowers/bushes. The average length of such nanorods was found in the range of 5-7 μm. The SEM images of ZnO NRs bushes between two Cu electrodes i.e., on bare PCB surface is shown in Fig. 2(b). Dense and interconnected ZnO with flowery morphology can be seen on etched part between the copper electrodes. Particularly growth of ZnO with flowery morphology can be observed on etched part between the copper electrodes and flowers/bushes are interconnected by overlapping rods via grain boundary contacts.

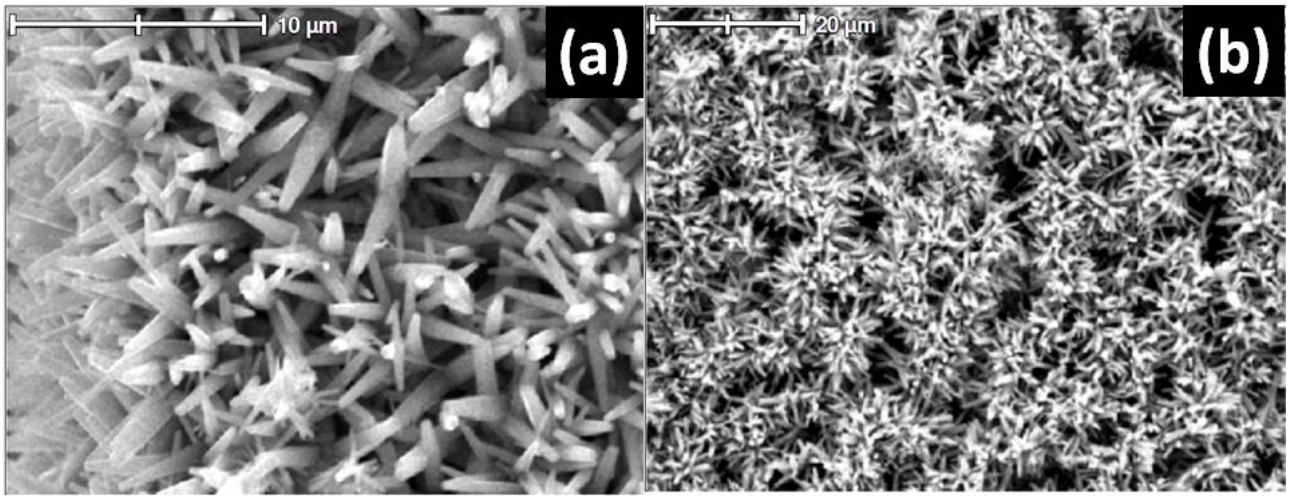

Fig. 2. SEM of the ZnO NRs (a) at the edge of copper electrode and (b) between the trenched electrodes.

Fig. 3 (inset) shows the Ultraviolet-Visible (UV-Vis) absorption spectrum of the ZnO. Optical band gap E_g was estimated using the Urbach model by fitting the absorption coefficient α to the equation $\alpha = A(h\upsilon - E_g)^{1/2}$, where A is a constant related to the material refractive index and the electron/hole masses, h is Plank constant and υ is frequency of light. Tauc plot, $(\alpha E)^2$ versus photon energy (Fig. 3) was used to estimate the optical band gap (E_g) of ZnO NRs which is ~ 3.17 eV. This corresponds to the absorption maximum at 390 nm and is consistent with reported values (Acosta-Osorno et al 2019).

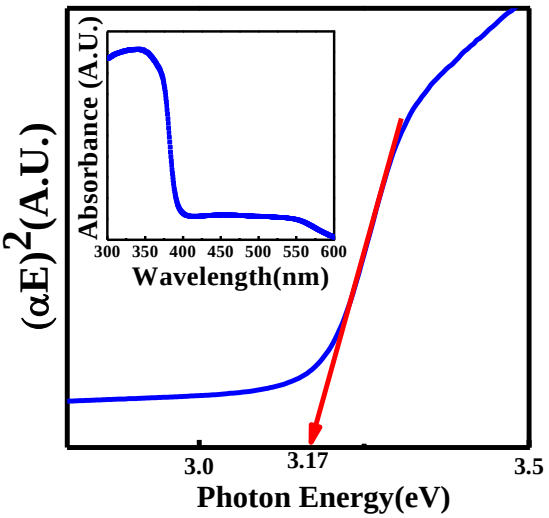

Fig. 3. Estimation of band gap energy from Tauc plot of $(\alpha E)^2$ versus E for the ZnO on Cu electrode. UV-Vis absorption spectrum is shown in the inset.

Room temperature photoluminescence spectrum of the embedded device using excitation wavelength of 325 nm is shown in Fig. 4. The strong PL emission peaks centered at 396.5 nm

and 410.5 nm represent the near band edge emissions and a weak broad band centered at 473.5 nm could be attributed to intrinsic deep level defects in ZnO crystals (Rasool et al 2020).

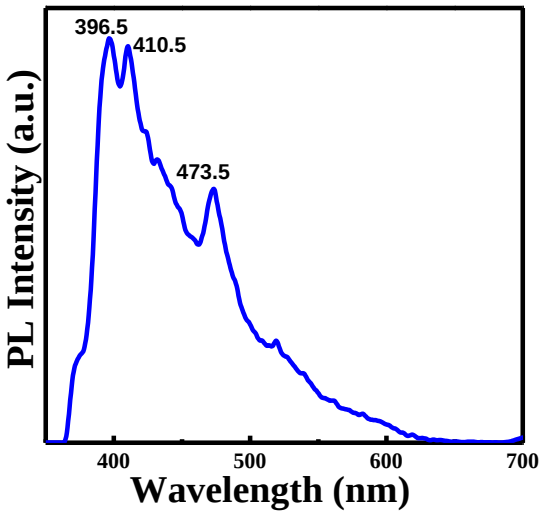

Fig. 4. Photoluminescence spectrum of ZnO NRs embedded device at excitation (λ_{ex}= 325 nm).

Photoelectrical characterization in the dark and under incident UV radiation is carried out for different current-voltages biases. A schematic view for the I-V measurements on ZnO NRs-embedded device is presented in Fig. 5 (a). In this case ZnO NRs are in contact with copper electrodes forming Cu-ZnO-Cu (MSM) junction contacts, therefore it is important to discuss the nature of this contacts. Fig. 5 (b) shows the energy band diagram of ZnO and Cu-metal before (a) and after (b) forming heterojunction. Metal-semiconductor junction can lead to Ohmic or Schottky type contacts depending on the work functions of both the metal and the semiconductor. If the work function of the metal (Φ_m) is greater than the work function of the semiconductor (Φ_s), a positive space charge region will be produced in the metal-semiconductor junction. Accordingly, the region will block the transfer of electrons between the metal and semiconductor. This contact type is defined as a Schottky contact. On the other hand, if Φ_m is lower than Φ_s, electrons will flow from the metal to the semiconductor. The contact type is defined as an Ohmic contact. In this case, a negative space charge region will appear at the interface. The high electron concentration will create a good conductivity in the metal-semiconductor junction. In our case, the work function of ZnO (5.2 eV) is larger than the work function of copper (4.65 eV) so the Cu-ZnO-Cu contact behave as ohmic contact. This means that electrons flow from the metal (Cu) to the semiconductor (ZnO) to lower their energies, until the positions of these Fermi energy levels get equalized to the same value. Therefore, valence and conduction bands of ZnO move relatively downwards to match Fermi levels (Ng and Sze 2006).

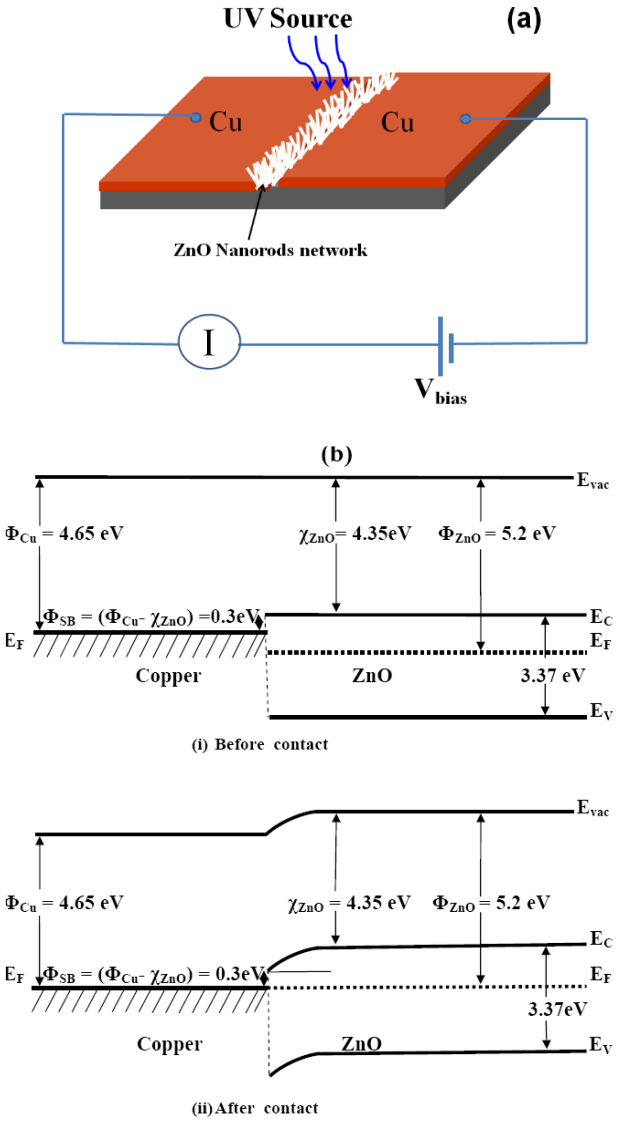

Fig. 5. (a) Schematic diagram for I-V measurements of the ZnO NRs embedded device and (b) Energy level diagram of Cu - ZnO (i) before MS contact and (ii) after the MS contact in thermal equilibrium.

Fig. 6 (a) shows current-voltage (I-V) response for ZnO NRs structure in the dark and as a function of UVC radiation peaked at λ~254 nm obtained from low-pressure Hg lamp. UV illumination intensity was effectively varied from 100 to 1885 μW/cm^2 by varying distance between UV source and the device. Current through the device was increased in discrete step of 5 μA to the maximum value of 100 μA. The plot shows that current rapidly increases for both positive and negative voltage after a threshold voltage bias. This nonlinear I-V characteristics in reversed and forward direction is analogous to varistor (back-to-back diode) characteristics.

More importantly, current through the device shows pronounced increase with intensity of UVC radiation as given in Fig. 6 (c). Here induced carrier density is proportional to generation of electron-hole pairs due to incident photon flux. These photo-generated electrons are transferred

from ZnO NRs to Copper electrodes increases the photo-current with an order of magnitude compared to values in the dark. Thus, the Cu-ZnO NRs-Cu (MSM) structure acts as a prototype UV photosensitive varistor.

It is well known that the nonlinearity in bulk ZnO varistor is a grain-boundary phenomenon where a barrier to electrons, especially in n-type ZnO, exists in the depletion region of adjacent grains. It has been understood that a double Schottky barrier between grain boundary region plays an important role for the appearance of the varistor type characteristic. Besides bulk and doped ZnO a non-linear I-V characteristic has been observed in high temperature annealed pulsed laser deposited ZnO thin films. Taking into consideration the past studies on bulk and thin film varistor, the nonlinear characteristic exhibited by the ZnO NRs structure is distinct and important as far as nano-rod based UV photo sensitive device is considered. Such characteristics is less known in the undoped ZnO NRs structures deposited using solution techniques. As discussed before in this case ZnO NRs growth takes place in the form of flower and are interconnected with each other forming multiple grain boundary contacts which is mainly responsible (back-to-back-diodes) to this varistor characteristics, the devices having a single ZnO contact involves a few grain-boundary contacts which generally reveal junction diode characteristics instead of a varistor characteristic.

It has been observed that Cu-ZnO-Cu junction is highly responsive to UV light. I-V characteristic is further analysed by plotting the photocurrent against incident UV intensity at 2 V bias values shown in Fig. 6 (b). The photocurrent increases from 25 to 100 μA when the UV light power increases from180 μW cm^{-2} to 1885 μW cm^{-2}, respectively. At low voltage bias the photocurrent increases approximately 4 times while at voltage bias of 10 V, photocurrent increases about 2 orders of magnitude which shows bias dependent photo-response functionality. The solid line fit in Fig. 6 (b) shows a strong linear relationship with a linear regression coefficient R^2 = 0.96, indicating that the present optoelectronic device can potentially be utilized as a quantitative UV sensor. Fig. 6 (c) shows the resistance measured against current increased in steps of 5 μA under dark conditions and UV illuminations of increasing intensity. It clearly indicates that the resistance decreases with increase in the UV light intensity. About two orders of magnitude decrease in resistance is observed as UV illumination intensity increases from 100 to 1885 μW cm^{-2}. We have repeated about ten such devices, checking each device at least 5 times. The photo-response of these devices was within ± 2 % error limit.

We have further explored the temperature dependent I-V characteristics at variable temperature conditions. Fig. 7 (a) indicates the temperature dependent I-V characteristics of the device in dark (without UV light). In the temperature regime 300 to 370 K, the device does not show much variation in electrical property. But on increasing the temperature from 370 to 430 K, device current increases from 2 to 100 μA at 5 V bias (see Fig. 7 (a)). Fig. 7 (b) indicates that there is no change in the resistance over the temperature range from 290-370 K. In the temperature range of 370 K to 430 K, the resistance decreases by 1-2 in orders of

magnitude, systematically as shown in Fig. 7(b). Due to thermionic effect, desorption of surface species such as oxygen ions (O^-, O^{2-}) from the surface of ZnO NRs is likely to be the main component which dominates above temperature of 370 K. Removal of oxygen from the surface results in a large increase in conductivity by increasing the electrons concentration contribute to conduction. As shown in Fig. 7 (c), in the regime of 290–370 K, log R linearly increases with 1/T. For instance, R decreases from 900 kΩ to 50 kΩ as temperature increases from 370 to 430 K. This linear behaviour of log *R* versus 1/*T* suggests that a thermally activated transport mechanism dominantly operates in that temperature regime thus the resistivity of the nanorods decreases, which indicates that ZnO exhibits negative temperature coefficient of resistance (NTCR) in high temperature regime (Li et al 2014).

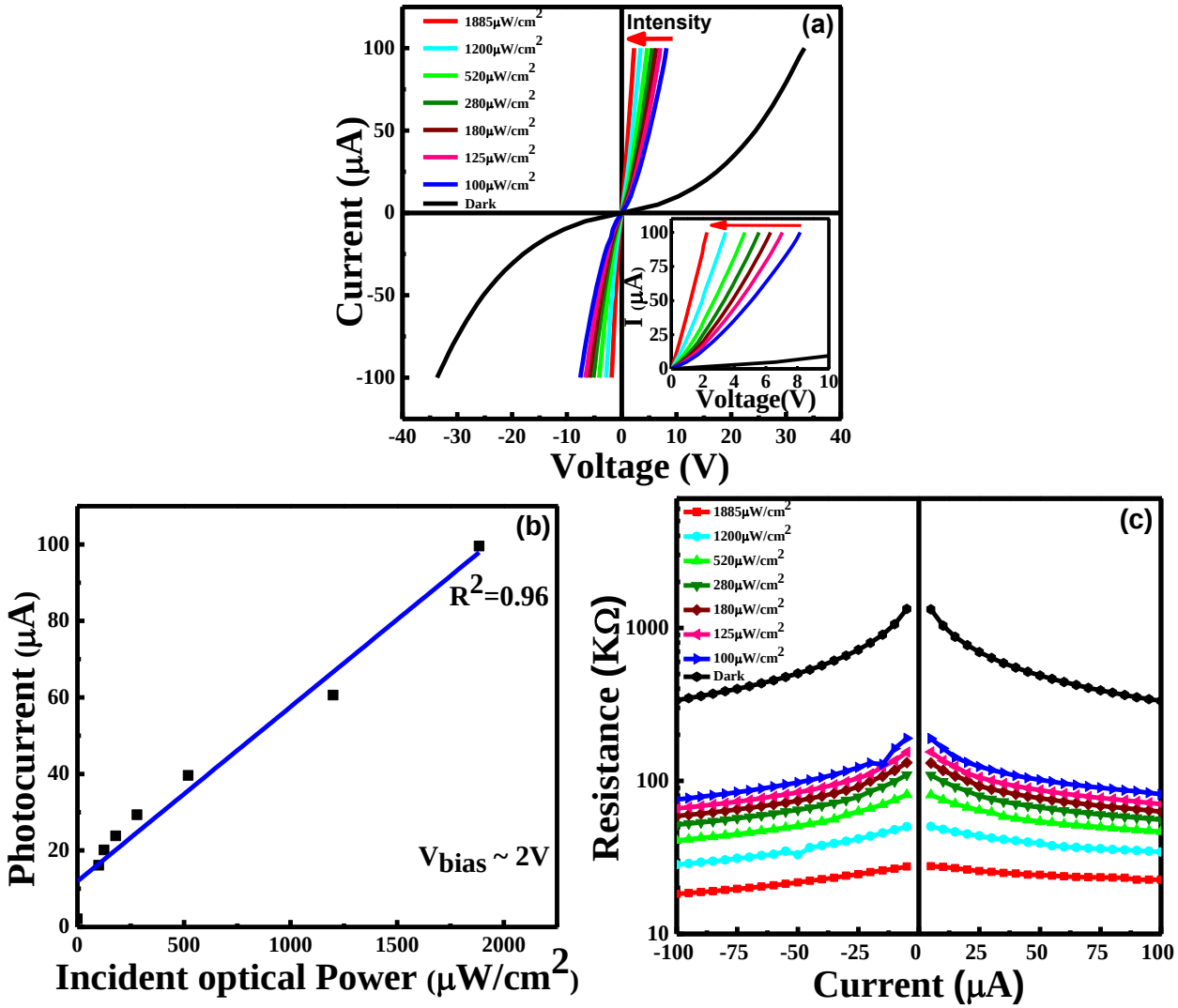

Fig. 6. (Colour online) (a) Current versus voltage curves of the ZnO NRs device in dark and when illuminated with UV (254 nm) photons of variable intensity. Inset shows a characteristic for V_{bias} for 0 to 10 V., (b) Photocurrent (the current increase under photon intensity) as a function of incident optical power at 2V bias and (c) Resistance against current measured in dark and under UV illumination of variable intensity.

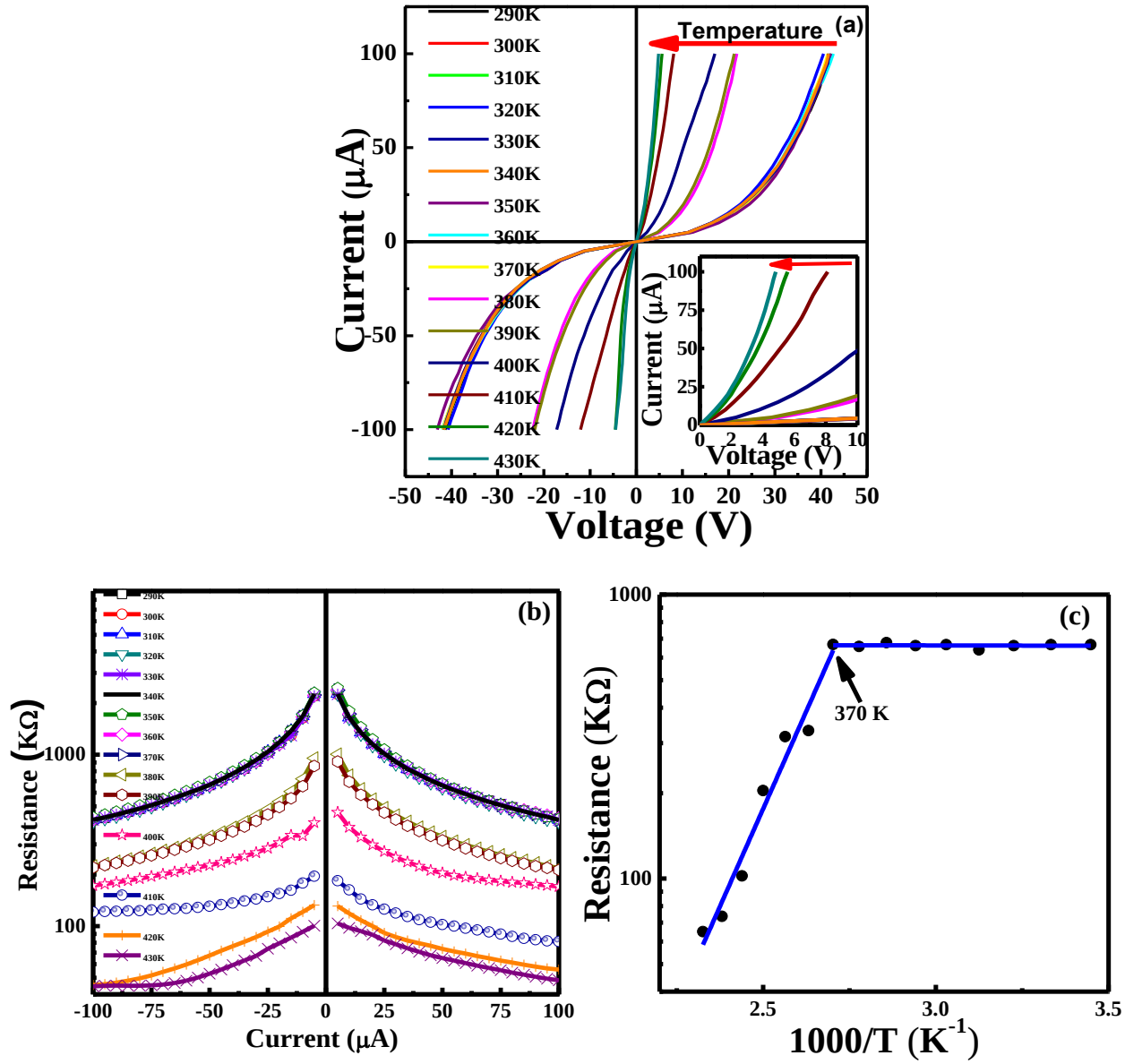

Fig. 7. (a) Current versus voltage curves of ZnO NRs embedded device under ambient temperature variation from 290 K to 430 K. Inset shows photoresponse between V_{bias} = ± 10 V, (b) Resistance against current measured in various temperature from 290 K to 430 K and (c) Resistance *vs* 1/T plot.

The time dependent photocurrent response was observed using Keithley source meter 2400 and controls via Lab-View program. Fig. 8 shows time dependent photocurrent response under UV illumination (λ ~ 254 nm). ZnO NRs are highly sensitive which increase photocurrent faster under UV illumination constant voltage of 5 V. The photoresponsivity of device is defined as ratio of photogenerated current to the incident illumination power however the sensitivity or the contrast ratio of sensors were calculated from the ratio of photocurrent to dark current (Singh and Park 2017). Compared with a dark current, the photocurrent under 254 nm UV light illumination increases by about four times. The photoresponsivity and sensitivity values of the

device is calculated to be 0.25 AW^{-1} and 4, respectively which also confirms that the responsivity and sensitivity behaves inversely to each other (Khayatian and Almasi 2019).

It has been observed that rise time is only ~ 4 min, but when UV light is turned off, the darkcurrent degenerates slowly and it takes ~ 30 minutes recovery time to reach its original state at room temperature (~ 23 ˚C). This is mainly due to multijunction of interconnected ZnO nanorods array.

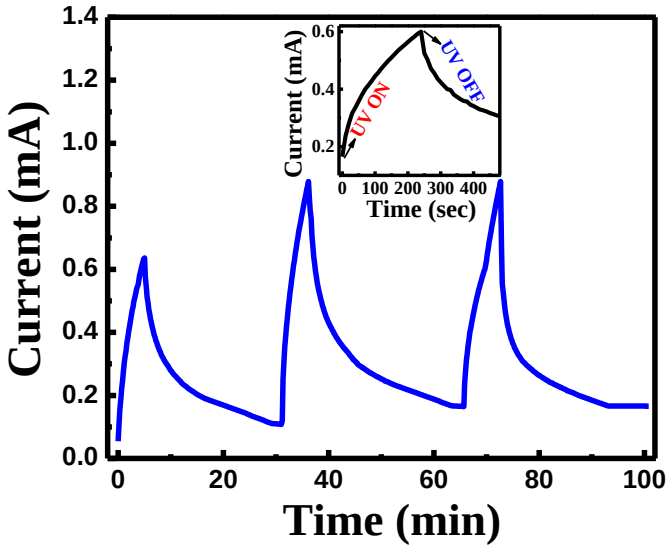

Fig. 8. Photo-switching in ZnO NRs embedded device copper electrodes at 5 V bias voltage.

A brief discussion on the mechanism of UV photo-response is in the following section. The loosely bound oxygen molecules at nanorod-air interface creates depletion region near the NRs surface by capturing free electrons from the n-type ZnO making negatively charged oxygen ions at the surface. [O_2 (g) $+e^- \rightarrow O_2^-(ad)$]. In our case upon exposure of UV photons of energy of 4.9 eV (λ ~ 254 nm), electron–hole pairs are generated, [$h\upsilon \rightarrow e^- + h^+$], the holes discharge the negatively charged adsorbing oxygen ions to photodesorb oxygen from the ZnO NRs surface and decrease the width of the depletion region. [$h^+ + O_2^-(ad) \rightarrow O_2(g)$], The electrons which are left behind contribute to decreasing resistance of the ZnO NRs . When the illumination is turned off, although holes quickly recombine with the electrons, there are still a lot of electrons left in ZnO NRs and oxygen readsorbs on the NRs surface, and it captures electrons, as a result current decreases slowly and it takes more time for returning the device to its initial state. This phenomenon of oxygen adsorption or re-adsorption takes place throughout the bulk of the materials. Thus, in device upon exposure of UV light, a lot of unpaired electrons are generated across NRs surface, which results in a rapid rise in the photocurrent whereas once the UV exposure is turned off it takes more time to drain out all those photogenerated electrons. This is the reason behind the faster current rise time and much slower photocurrent decay (Meng and Li, 2020, Rasoo et al 2020).

Conclusions:

In summary, we report growth of highly densed ZnO NRs array in trenched Copper electrodes by facile open aqueous solution deposition method. ZnO NRs embedded in metal-semiconductor-metal junction exhibit excellent UV-photoresponsivity. This device shows stable photoresponse below 370 K. Above 370 K, temperature dependent electrical properties show negative temperature coefficient of resistance effect. The ZnO NRs embedded on trenched copper electrodes grown by facile solution technique, is low cost and easy for bulk manufacturing and exhibits multifunctional optoelectronic photodetection property.

Acknowledgements:

Authors would like to thank emeritus Prof. Dr. Satishchandra Ogale (IISER, Pune) for his valuable guidance throughout the work. Authors also appreciate Mr. Prabhat Jha for his help during experiments and Mr. Sanjay Harchikar (Arklite Innovation system, Pune) for providing UV lamp and detector. Authors would like to acknowledge Department of Physics, Savitribai Phule Pune University, Pune for providing characterisation facilities. Authors would like to acknowledge seed money support from Deccan Education Society's Fergusson College (Autonomous) Pune.

References:

Acosta-Osorno M, Alcántara-Iniesta S, Alvarado J, Young CD, Mejía I, García M, Ramos-Serrano J R and Juarez-Díaz G (2019) Characterization of ZnO thin films obtained by ultrasonic spray pyrolysis for application in UV photoconductive detectors. Mater. Res. Express. 6:116450.

Ahmad R, Tripathy N, Jung D and Hahn YB (2014) Highly sensitive hydrazine chemical sensor based on ZnO nanorods field-effect transistor. Chem. Commun. 50: 1890-1893.

Ashraf S, Jones AC, Bacsa J, Steiner A, Chalker PR, Beahan P, Hindley S, Odedra R, Williams PA and Heys PN (2011) MOCVD of vertically aligned ZnO nanowires using bidentate ether adducts of dimethyl Zinc. Chem. Vap. Depos. 17: 45-53.

Bavelis K, Gjonaj E, Weiland T, Elektromagnetischer T, Darmstadt TU (2014) Synthesis of ZnO nanowires on Si substrate by thermal evaporation method without catalyst : Structural and optical properties. Adv. Radio Sci.12: 29-34.

Brillson L J and Lu Y (2011) ZnO schottky barriers and ohmic contacts. J. Appl. Phys. 109: 121301.

Chang SL, Park MC, Kuang Q, Deng Y, Sood AK, Polla DL and Wang ZL (2007) Giant enhancement in uv response of zno nanobelts by polymer surface-functionalization. J. Am. Chem. Soc. 129: 12096-12097.

Chen L, Cui J, Sheng X, Xie T, Xu T and Feng X (2017) High-performance photoelectronic sensor using mesostructured ZnO nanowires. ACS Sensors 2: 1567-1572.

Consonni V, Briscoe J, Kärber E, Li X and Cossuet T (2019) ZnO nanowires for solar cells: a comprehensive review. Nanotechnology 30: 362001.

Deo M, Shinde D, Yengantiwar A, Jog J, Hannoyer B, Sauvage X, More M and Ogale S

(2012) Cu_2O/ZnO hetero-nanobrush: Hierarchical assembly, field emission and photocatalytic properties. J. Mater. Chem. 22: 17055-17062.

Farhat OF, Halim MM, Ahmed NM, Oglat AA, Abuelsamen AA, Bououdina M and Qaeed M A (2017) A study of the effects of aligned vertically growth time on ZnO nanorods deposited for the first time on Teflon substrate. Appl. Surf. Sci. 426: 906-912.

Huang CC, Pelatt BD and Conley JF (2010) Directed integration of ZnO nanobridge sensors using photolithographically patterned carbonized photoresist. Nanotechnology 21: 195307.

Huang MH, Mao S, Feick H, Yan H, Wu Y, Kind H, Weber E, Russo R and Yang P (2001) Room-temperature ultraviolet nanowire nanolasers. Science 292: 1897-1899.

Hwang JD, Jiang CI and Hwang SB (2020) *p*-NiO/*n*-ZnO heterojunction photodiodes with an MgZnO/ZnO quantum well insertion layer. Mater. Sci. Semicond. Process. 105: 104711.

Jejurikar SM, Banpurkar AG, Limaye AV, Date SK, Patil SI and Adhi KP (2006) Structural , morphological , and electrical characterization of heteroepitaxial ZnO thin films deposited on Si (100) by pulsed laser deposition : Effect of annealing (800 °C) in air. J. Appl. Phys. 99: 014907.

Kao CY, Hsin CL, Huang CW, Yu SY, Wang CW, Yeh PH and Wu WW (2012) High-yield synthesis of ZnO nanowire arrays and their opto-electrical properties. Nanoscale 4:1476-1480.

Khayatian S and Almasi R (2019) Three - dimensional ZnO nanorods growth on ZnO nanorods seed layer for high responsivity UV photodetector. Appl. Phys. A. 125:1-13.

Ko Y H, Nagaraju G and Yu J S (2015) Fabrication and optimization of vertically aligned ZnO nanorod array-based UV photodetectors via selective hydrothermal synthesis. Nanoscale Res. Lett. 10: 323.

Kumar M, Kim J and Wong CP (2019) Transparent and flexible photonic artificial synapse with piezo-phototronic modulator: Versatile memory capability and higher order learning algorithm. Nano Energy 63: 103843.

Li G, Zhang J and Hou X (2014) Temperature dependence of performance of ZnO-based metal-semiconductor- metal ultraviolet photodetectors. Sens. Actuators, A Phys. 209: 149-153.

Li J, Zhang Q, Peng H, Everitt H O, Qin L and Liu J (2009) Diameter-controlled vapor−solid epitaxial growth and properties of aligned ZnO nanowire arrays. J. Phys. Chem. C 113: 3950–3954.

Lyu SC, Zhang Y and Lee CJ (2003) Low-temperature growth of ZnO nanowire array by a simple physical vapor-deposition method. Chem. Mater. 15: 3294–3299.

Mahan GD, Levinson LM and Philipp HR (1978) Single grain junction studies of ZnO varistors—Theory and experiment. Appl. Phys. Lett. 33: 830–832.

Mahan GD, Levinson LM and Philipp HR (1979) Theory of conduction in ZnO varistors. J. Appl. Phys. 50: 2799-2812.

Mandal L, Deo M, Yengantiwar A, Banpurkar A, Jog J and Ogale S (2012) A quasi-liquid

iontronic-electronic light-harvesting hybrid photodetector with giant response. Adv. Mater. 24: 3686-3691.

Meng J and Li Z (2020) Schottky-contacted nanowire sensors. Adv. Mater. 32: 2000130.

Ng KK and Sze SM (2006) Physics of semiconductor devices, (3rd eds) Hoboken, New Jersey: John Wiley & Sons, Inc.

Özgür Ü, Alivov YI, Liu C, Teke A, Reshchikov MA, Doğan S, Avrutin V, Cho SJ and Morkoç H (2005) A comprehensive review of ZnO materials and devices. J. Appl. Phys. 98:41301.

Postels B, Bakin A, Wehmann H H, Suleiman M, Weimann T, Hinze P and Waag (2008) Electrodeposition of ZnO nanorods for device. A Appl. Phys. A 91: 595-599.

Rasool A, Santhosh Kumar MC, Mamat MH, Gopalakrishnan C and Amiruddin R (2020) Analysis on different detection mechanisms involved in ZnO-based photodetector and photodiodes. J. Mater. Sci. Mater. Electron. 31: 7110–7113.

Resmini A, Tredici IG, Cantalini C, Giancaterini L, De Angelis F, Rondanina E, Patrini M, Bajoni D and Anselmi-Tamburini U (2015) A simple all-solution approach to the synthesis of large ZnO nanorod networks. J. Mater. Chem. A 3: 4568–4577.

Singh S and Park S (2017) Optik Fabrication and properties of ZnO nanorods based MSM UV detectors on silicon substrates. Opt. - Int. J. Light Electron Opt. 137: 96-100.

Sönmezoğlu S, Eskizeybek V, Toumiat A and Avcı A (2014) Fast production of ZnO nanorods by arc discharge in de-ionized water and applications in dye-sensitized solar cells. J. Alloys Compd. 586: 593–599.

Su YK, Peng SM, Ji LW, Wu CZ, Cheng WB and Liu CH (2010) Ultraviolet ZnO nanorod photosensors. Langmuir 26: 603-606.

Umar A, Ra H, Jeong J, Suh E and Hahn Y (2006) Synthesis of ZnO nanowires on Si substrate by thermal evaporation method without catalyst : Structural and optical properties. Korean J. Chem. Eng. 23: 499-504.

Wei TY, Yeh PH, Lu SY and Wang ZL (2009) Gigantic enhancement in sensitivity using schottky contacted nanowire nanosensor. J. Am. Chem. Soc. 131: 17690–17695.

Yengantiwar A, Sharma R, Game O and Banpurkar A (2011) Growth of aligned ZnO nanorods array on ITO for dye sensitized solar cell. Curr. Appl. Phys. 11: S113-S116.

Zhai T, Li L, Ma Y, Liao M, Wang X, Fang X, Yao J, Bando Y and Golberg D (2011) One-dimensional inorganic nanostructures: synthesis, field-emission and photodetection. Chem. Soc. Rev. 40: 2986.